Electron spin resonance of doped chalcogenide nanotubes

Denis Arčon,[1,2] Andrej Zorko,[1] Pavel Cevc,[1] Aleš Mrzel,[1] Maja Remškar,[1] Robert Dominko,[3] Miran Gaberščček,[3] and Dragan Mihailović[1]

[1]*Institute Jožef Stefan, Jamova 39, 1000 Ljubljana, Slovenia*

[2]*Faculty of Mathematics and Physics, University of Ljubljana, Jadranska 19, 1000 Ljubljana, Slovenia*

[3]*National Chemistry Institute, Hajdrihova 19, 1000 Ljubljana, Slovenia*

(Received 13 September 2002; revised manuscript received 26 November 2002; published 31 March 2003)

X-band ESR of lithium doped MoS_2 nanotubes is reported for temperatures between room temperature and 4 K. Two distinct ESR components were observed: a narrow component with a linewidth of about 4 G and a broad component with a linewidth of more than 800 G. The broad ESR component is attributed to Mo *d*-orbital-derived conducting band of MoS_2 nanotubes. The large weakly temperature-dependent ESR spin susceptibility of charged MoS_2 nanotubes is thought to reflect strong electronic correlations and one-dimensional electronic structure with the presence of van Hove singularities in the density of states. The broad ESR component is discussed in terms of conducting electrons coupled to defects and in terms of random-exchange Mo Heisenberg chain model. The narrow component is suggested to be due to the formation of small spin clusters.

DOI: 10.1103/PhysRevB.67.125423 PACS number(s): 61.46.+w, 76.30.−v

I. INTRODUCTION

The study of carbon nanotubes has been an extremely active field since their discovery by Iijima.[1] The research was stimulated both from the fundamental physics point of view as well as for potential application. The interest for the fundamental physics lays in the fact that nanotubes are a good realization of a one-dimensional (1D) systems. It is known that the usual Fermi-liquid theory, based on a quasiparticle picture, breaks down in one dimension and so the electronic properties of 1D interacting fermions may be described within Luttinger liquid theory.[2,3] Several experiments on carbon nanotubes probing charge dynamics[4–6] were interpreted in terms of this theory. On the other hand, nanotubes have also a considerable application potential. A number of groups have explored the possibility of using carbon nanotubes as host materials for energy storage.[7–10] High electrochemical reactivity and inherent porosity of carbon nanotubes structures lead to relatively high charge capacities of the tested materials. Reversible capacity depends on the quality and morphology of the used material and can be increased from LiC_6 to LiC_3 after chemical etching of carbon nanotubes.[11] Due to the vast diversity of carbon nanotubes there is at the moment no definite consensus on how good carbon nanotubes can be as a basic material for energy storage.

However, synthesis of fullerenelike objects and nanotubes is possible also from other inorganic layered materials. For instance boron nitride nanotubes were synthesized[12] and many of the experiments performed on carbon nanotubes were repeated on this system as well.[13] Another class of inorganic nanostructures represent vanadium-oxide nanotubes,[14] whose electrochemical activity was recently tested[15] giving a promising charge capacity of 140 mAh/g.

Still another family of inorganic nanostructures is based on dichalcogenide materials. Fullerenelike nanoparticles and tubelike particles[16–19] were reported and even used as a hydrogen storage material.[20] All these materials suffered from the same problem as carbon nanotubes: low yield, wide range of diameters and thus very diverse physical or chemical properties. A breakthrough in overcoming these problems has been made recently by the synthesis of self-assembled single-wall subnanometer-diameter molybdenum disulfide tubes ($n$$MoS_2$).[21] A high-resolution transmission electron microscopy investigation revealed a hexagonal close packing of identical nanotubes, where the center-to-center distance between two tubes is 0.96 nm.[21] The unit cell of the hexagonal close-packed nanotubes within bundle was determined to be 0.40 nm along the bundle axis. A detailed structure of individual nanotubes is not precisely known at the moment. However, the proposed structure consisting of sulfur-molybdenum-sulfur cylinders (Fig. 1) is a good approximation. Using the nomenclature introduced to describe carbon nanotubes[22] the proposed structure of $n$$MoS_2$ nanotubes would correspond to (3,3) armchair nanotubes. We also note

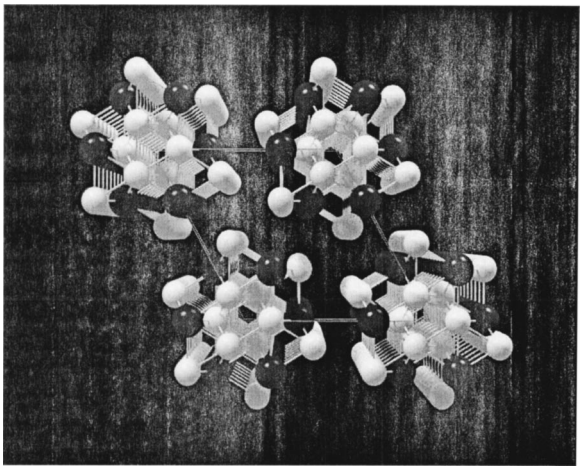

FIG. 1. Schematic structure of hexagonal close packing of $n$$MoS_2$. Yellow spheres represent sulphur atoms, while larger blue spheres represent molybdenum atoms. Please note two different intercalations sites for Li^+ ions: larger interstitial channels between the $n$$MoS_2$ and much smaller channels inside individual $n$$MoS_2$.

that the presence of iodine has been identified in the trigonal voids between the nanotubes.[21] It seems that the presence of iodine is crucial for the stability of bundles of $n\mathrm{MoS_2}$ and that removing iodine dramatically decrease the size of $n\mathrm{MoS_2}$ bundles. The correct stoichiometry of our samples is thus $\mathrm{MoS}_y\mathrm{I}_z$ with $y\sim 2$ and $z\sim 0.33$. Regardless of these uncertainties in the exact structure and stoichiometry we will use the nomenclature $n\mathrm{MoS_2}$ throughout this paper to name our nanotubes.

In this contribution we report on the study of the low-temperature electronic properties of electrochemically doped $n\mathrm{MoS_2}$ with Li. Our starting point relied on two facts: first, many chalcogenides have been successfully used for energy storage in the past[23,24] and second the porous structure of $n\mathrm{MoS_2}$ with the sizes of channels larger than 1.1 Å offers a good possibility for intercalation chemistry. Basically we have found that large amounts of Li^+ ions can be intercalated into the channels between the individual $n\mathrm{MoS_2}$ nanotubes. Intercalation goes mainly through one-dimensional diffusion of Li^+ ions into the host structure donating an electron to the $n\mathrm{MoS_2}$ nanotubes. It seems that the Li^+ ion intercalation leads to a formation of many defects, which effectively decrease the $n\mathrm{MoS_2}$ tube length as compared to the electron correlation length. These defects, which can be either topological or paramagnetic or even a result of inhomogeneous doping, determine the low-temperature electronic properties of doped $n\mathrm{MoS_2}$ nanotubes. They may even reflect partial amorphization of the doped electrode material and be responsible for the relatively large irreversible losses during the first charging cycle.

II. EXPERIMENTAL

A. Electrochemical Li doping

Single-wall $n\mathrm{MoS_2}$ were grown by a catalyzed transport method using $\mathrm{C_{60}}$ as a growth promoter in the reaction.[21] Transported material was than removed from a quartz tube and checked with electron microscopy.

Several different batches of $n\mathrm{MoS_2}$ nanotube swatches were used for the electrochemical Li doping. The working electrodes were prepared by mixing as-grown $n\mathrm{MoS_2}$ nanotube bundles or dispersed $n\mathrm{MoS_2}$ nanotube bundles[25] with 10 wt.% of sulphonated polyaniline (for improved electrical contact).[26,27] The slurry was spread over a copper substrate, partially dried, pressed and then again dried in vacuum at 100°C for at least 8 h, before they are transferred to the glove box (<1 ppm $\mathrm{H_2O}$). It is important to control the water content during and after the intercalation of the $\mathrm{MoS_2}$ systems as it is well known that a water uptake by intercalated alkali metals can easily take place.[28] In order to avoid this effect we strictly handled our samples in an inert atmosphere with very low $\mathrm{H_2O}$ content at all stages of sample preparation.

Electrochemical lithium insertion into $n\mathrm{MoS_2}$ nanotube bundles was carried out in a laboratory-made three-electrode cell.[29] The cell body was made of polypropylene, whereas the electrode holders, which also served as contacts, were made from stainless steel. The working electrode and counter lithium metal electrode were held apart with two separators (Celgard No. 2402) between which a thin strip of lithium serving as a reference electrode was positioned. Before assembling, the working electrode and separators were soaked with electrolyte (1M $\mathrm{LiClO_4}$ solution in propylene carbonate). Electrochemical measurements were recorded using an EG&G 283 electrochemical interface at constant current, typically 0.025 mA. The geometric surface area of the working electrode was always 0.5 $\mathrm{cm^2}$ containing ≈ 1 mg of active material.

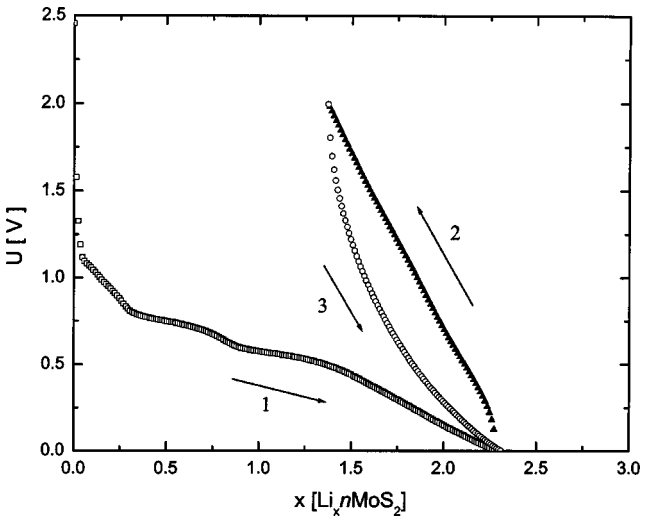

FIG. 2. Typical charge or discharge curves measured in $n\mathrm{MoS_2}$.

Typical charge or discharge curves for $n\mathrm{MoS_2}$ samples are shown in Fig. 2. The charge capacity in a typical $n\mathrm{MoS_2}$ sample is in the first cycle ≈ 385 mAh/g and corresponds to an intercalation of about 2.3 Li per $\mathrm{MoS_2}$.[26,27] This is ~ 2 times higher than in layered $\mathrm{MoS_2}$ with the same cell configuration, where—in agreement with previously published data[30,31]—we could intercalate up to ~ 1 mole of Li per one mole of $\mathrm{MoS_2}$.

B. ESR measurements

After electrochemical doping, the $\mathrm{Li}_x n\mathrm{MoS_2}$ sample was scratched from the substrate in a glove box and sealed into an ESR quartz tube. Continuous wave (cw) ESR measurements were performed on a Varian dual resonator with a reference sample in the second resonator to account for the slight changes in the Q factor during the measurements. In all cw experiments a modulation field $H_{mod}=1$ G and $\nu_{mod}=100$ kHz were used. The temperature was stabilized within 0.2 K in a continuous flow cryostat ESR 900. To estimate the ESR spin susceptibility $\mathrm{Cu(SO_4)_2\cdot 5H_2O}$ has been used as a standard sample.

Pulsed ESR experiments were performed on a Bruker E580 spectrometer equipped with cylindrical dielectric resonator md5. A typical $\pi/2$ pulse width used in these experiments was 12 ns. To record echo decay intensity a $\pi/2-\pi$ separation pulse τ was incremented from 160 ns in 1024 experiments with 4 ns increments. Phase cycling was used to remove the unwanted ringing in our signal.

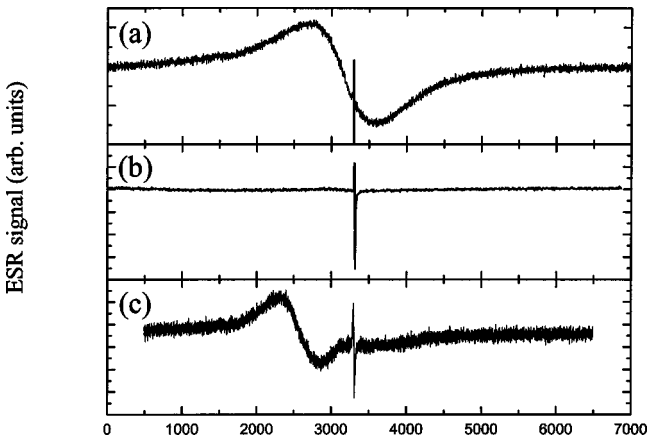

FIG. 3. (a) Room-temperature *X*-band ESR spectrum in Li_xnMoS_2 sample ($x\sim2.3$). (b) For comparison only a narrow component is measured in dispersed Li_xnMoS_2 samples. (c) Room-temperature *X*-band ESR spectrum in layered Li_xMoS_2 sample ($x\sim1$).

III. RESULTS

In this section we present ESR results as a function of sample preparation, as a function of the exposure of the sample to air and finally as a function of temperature.

A. Room-temperature spectrum

As prepared $nMoS_2$ samples show no ESR signal at room temperature. When $nMoS_2$ is electrochemically doped with Li, a strong ESR signal appears. A typical room-temperature *X* band cw ESR spectrum taken in one of the Li_xnMoS_2 samples ($x\sim2.3$) is shown in Fig. 3(a). The spectrum consists of two quite different components: (i) a narrow component with a *g*-factor $g_1=2.0029$ and with a linewidth of few Gauss and (ii) a broad component with a *g*-factor $g_2\sim2.15$ and linewidth of more than 800 G. For comparison also room-temperature spectrum taken at *Q* band (35 GHz) has been measured. The linewidth of both components of the cw ESR spectra are comparable (although slightly larger for a broad component in *Q* band) with the values taken in the *X* band (9.6 GHz).

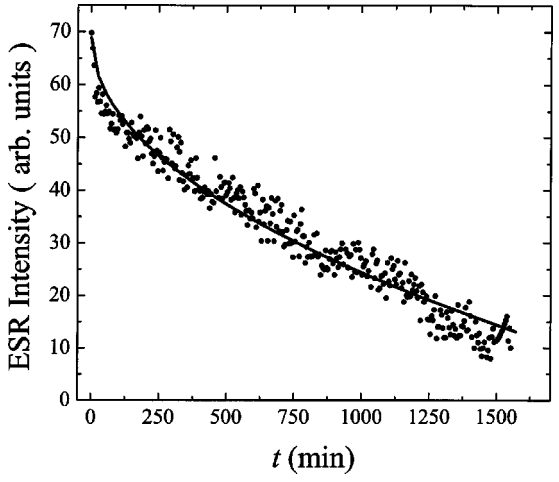

FIG. 4. Decay of the intensity of the *X*-band ESR signal in Li_xnMoS_2 sample ($x=2.3$) after its exposure to air. Solid line represents a fit to Eq. (1).

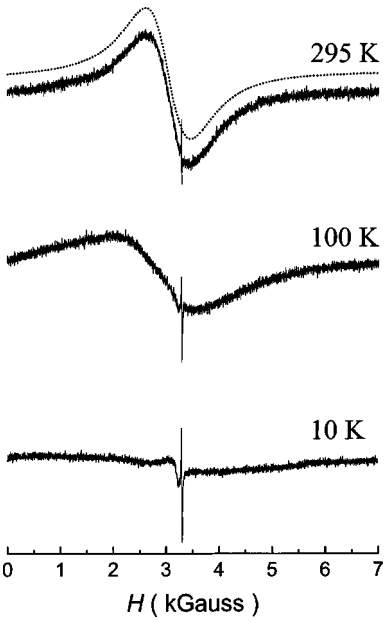

FIG. 5. The temperature evolution of the *X*-band ESR spectra in $Li_{2.3}nMoS_2$ powder sample. A dotted line, which is plotted over the 295-K spectrum is a simulation of a broad ESR component with a Lorentzian lineshape. On a 10-K spectrum one can see also a third line with a center at 3184 G, whose appearance is very irregular (found in only few samples) and thus attributed to the impurities.

The relative intensities of the two components vary somewhat from sample to sample. A very likely reason for this variation is different sample pretreatment and quality. For instance, doped samples prepared from dispersed $nMoS_2$ show only a narrow ESR component [Fig. 3(b)] while the broad ESR component is strongly suppressed. This is in agreement with the electrochemical results which suggested that in dispersed samples very little Li has been intercalated (less than 0.5 of Li per MoS_2 unit) and even this little quantity of Li is then largely irreversibly lost. Presumably Li chemically reacts with iodine in the first doping cycle.

We also measured the ESR signal of a Li doped layered MoS_2 sample. A room-temperature ESR spectrum of this sample is shown on Fig. 3(c). Again we found in the ESR spectrum two very different ESR components. The linewidth of the broad ESR component in layered Li_xMoS_2 is around 500 G and its *g* factor is about 2.52 and somehow resembles the broad ESR component measured in Li_xnMoS_2. The linewidth and the *g* factor of the narrow component are similar in both cases.

Another line appears at very low temperatures in some of the samples—although not in all Li_xnMoS_2—with a center at 3184 G, a linewidth of about 150 G and a lineshape characteristic of powder *g*-factor broadening (see spectrum at 10 K on Fig. 5). The temperature dependence of its ESR intensity shows a typical Curie-like dependence. The appearance of this line is very irregular and it has been found only in two Li_xnMoS_2 samples. We therefore believe that this line is not intrinsic and it will not be discussed further.

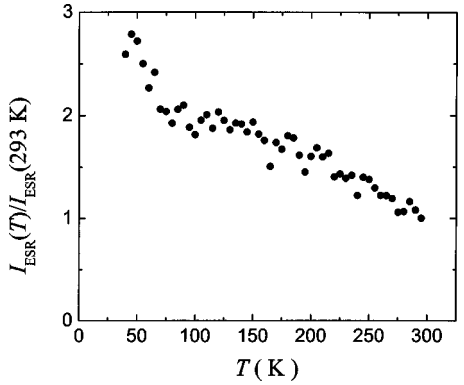

FIG. 6. The temperature dependence of the ESR intensity of the broad ESR component. Please note large error bar as consequence of large linewidth as well as only a weak temperature dependence of the ESR susceptibility.

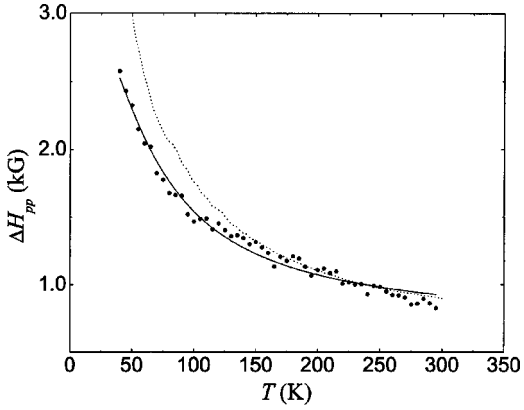

FIG. 7. Temperature dependence of the ESR linewidth of the broad ESR component in $Li_{2.3}nMoS_2$. Points represent experimental data, dotted line is a fit to Eq. (2), while solid line is a fit to Eq. (3).

B. Air sensitivity

To test air sensitivity of $Li_{2.3}nMoS_2$ samples we opened the quartz ESR tube and exposed the sample to air. The ESR signal was then measured as a function of exposure time. We noted that the positions and the linewidths of the two ESR components did not change significantly during the whole experiment. However, the total intensity of the ESR signal did change as shown on Fig. 4. The intensity of the ESR signal quite rapidly decreased for about 10% during the first few minutes. Later on the ESR intensity decayed very slowly with time as we still managed to detect ESR signal even after several hours. Surprisingly, the degradation of the ESR signal goes exclusively on the account of the broad ESR component, while the narrow ESR line remained almost unchanged.

C. Temperature dependence of the broad component of the ESR spectrum

We attribute the broad ESR component to be intrinsic to doped $nMoS_2$ as it does not vary substantially from sample to sample and because of its dominant intensity. The room temperature ESR signal is nearly symmetric [Figs. 3(a) and 5]. We note, however, a small shoulder on the low-field side of the spectra, which on cooling becomes even more pronounced (see for instance 100-K ESR spectrum on Fig. 5). This shoulder makes the ESR lineshape slightly asymmetric over the entire temperature interval. Without this shoulder the ESR line can be to a good approximation fitted with a Lorentzian lineshape (dotted line in Fig. 5). The g factor of the broad component of the ESR line is $g_2 \sim 2.15$. This value is far from the free-electron value 2.0023 and suggests considerable spin-orbit coupling.

The measured ESR susceptibility of the broad ESR component in $Li_{2.3}nMoS_2$ powdered sample shows only a weak temperature dependence in the temperature range between 300 K and 50 K (Fig. 6). The ESR intensity increases by a factor of 2 on cooling from room-temperature to 50 K and does not follow a Curie-like temperature dependence. At this point we would like to mention two important observations. First, the determined values of the ESR susceptibility are the subject of large error bars due to the large linewidth and slightly asymmetric ESR lineshape. In fact, below 40 K due to the extreme broadening of the ESR line it was impossible to get even an estimate of the ESR susceptibility and it may well be, that the increase of the ESR susceptibility below 60 K shown on Fig. 6 is an artifact. Second, the magnitude of the ESR susceptibility is very large. We tried to determine the absolute value of the ESR susceptibility by comparing our signal to a standard sample and obtained a room-temperature value 6×10^{-3} emu/mol. Again, this value is uncertain for several reasons: ill defined mass of the $Li_{2.3}nMoS_2$ sample, which may contain also some residual solvent or electrolyte, and difficulties with the analysis of the broad ESR line. Nevertheless, the obtained value of the ESR susceptibility represents a good estimate of the order of magnitude.

The temperature dependence of the peak-to-peak ESR linewidth of the broad component measured in powdered $Li_{2.3}nMoS_2$ is shown in Fig. 7. The linewidth on cooling increases from about 800 G at room temperature to 2600 G at 40 K. Below that temperature the line becomes so broad that it is almost impossible to reliably analyze the measured spectra.

D. Temperature dependence of the narrow component of the ESR spectrum

In this section we describe the temperature dependence of the narrow ESR component of the Li_xnMoS_2 ESR spectra. We measured ESR spectra only in a narrow field sweep around the center of the narrow ESR component and then subtracted the contribution of the broad component. Representative spectra of the narrow ESR component are shown in Fig. 8. Here we would like to mention that the details of the narrow ESR component vary somewhat from sample to sample. The g factor is the same in all measured samples, but the room-temperature linewidth slightly varies. Nevertheless the overall temperature dependence of the narrow ESR component was similar in all cases.

The g-factor value for the narrow component is $g = 2.0029$ and suggests nearly free electronic states with a

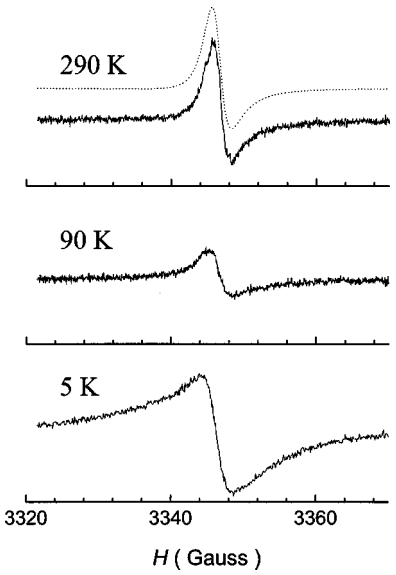

FIG. 8. The temperature evolution of the narrow component of the ESR spectra in $Li_{2.3}nMoS_2$ nanotubes. Dotted line superimposed over the 290 K spectrum is a calculated Dysonian lineshape. Please note the gradual change from the Dysonian lineshape at room-temperature to more symmetric line at low temperatures.

very small spin-orbit interaction. The *g*-factor value of the narrow component is temperature independent between the room temperature and 5 K.

The room-temperature ESR line is strongly asymmetric and resembles a Dyson-like lineshape[32] usually found in metallic samples. An attempt to fit the 290 K spectrum with a Dyson lineshape is shown in Fig. 8. The agreement is excellent. However, on cooling bellow 100 K the agreement with the experiment becomes very poor as the measured ESR spectra changes gradually from Dyson-like lineshape at temperatures above 100 K to more symmetric lineshape at temperatures below 100 K (Fig. 8).

The temperature dependence of the intensity of the ESR signal, which is proportional to the electronic spin susceptibility χ_0 (this is not strictly true if the line is Dysonian), confirms changes suggested by the temperature evolution of the ESR lineshape. The ESR intensity first marginally decreases with decreasing temperature for about 10%. The decrease of the intensity of the ESR signal between room temperature and 100 K is rather small and is within the error bar of the experiment. At around 100 K the ESR intensity reaches its minimum and then it begins to grow quite rapidly on further cooling as the temperature approaches 5 K [Fig. 9(a)] exhibiting a Curie-like temperature behavior. The slight variation of the ESR intensity between room temperature and 100 K cannot be accounted for the small variation of the resonator *Q* factor as this has been checked and ruled out by independent measurements of the standard sample in the second resonator.

The temperature dependence of the linewidth of the ESR signal shows only a gradual increase with decreasing temperature [Fig. 9(b)]. We have not noticed any dramatic changes around 100 K, i.e., in the temperature interval where

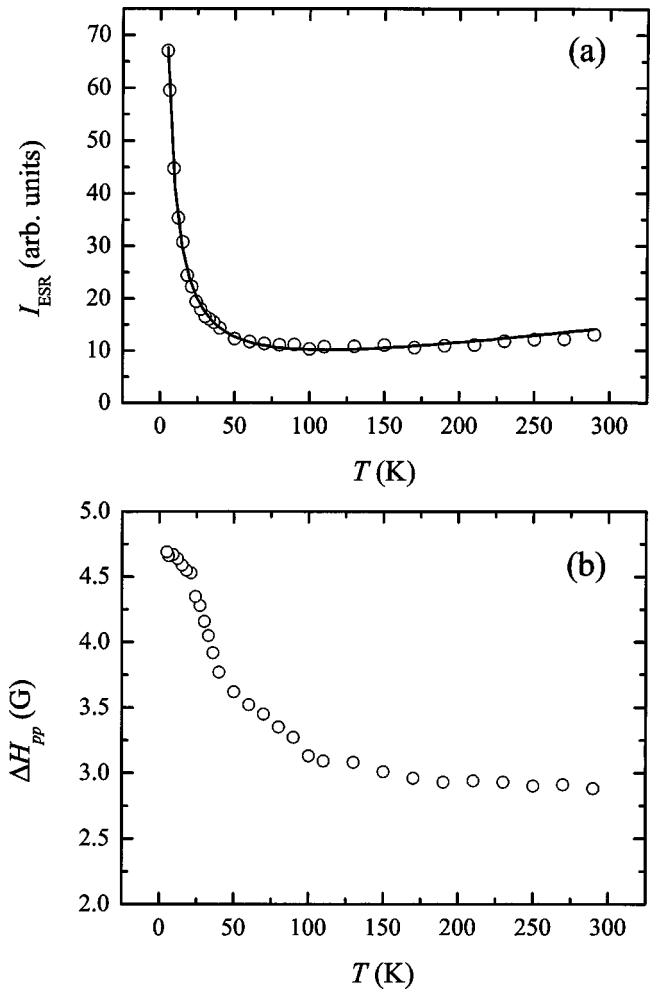

FIG. 9. The temperature dependence of (a) the ESR intensity and (b) the ESR linewidth of the narrow component of the ESR signal in $Li_{2.3}nMoS_2$. The solid line is a fit of the ESR intensity to Eq. (6).

the ESR lineshape and ESR intensity change their character. The linewidth simply monotonically increases with decreasing temperature from the room-temperature value of $\Delta H_{pp} = 2.8$ G to $\Delta H_{pp} = 4.7$ G at 5 K.

The observation of the spin-echo in Li_xnMoS_2 proves that the narrow component of the ESR line is inhomogeneously broadened at low temperatures. The measured decay of the electron-spin echo is shown in Fig. 10. A phase-memory time extracted from the monoexponential fit of the echo decay is $T_M = 173$ ns. A modulation superimposed on the top of the echo decay is clearly visible. This modulation is known as a electron-spin-echo-envelope-modulation.[33,34] A Fourier transform of the modulation (after the monoexponential decay of the echo has been subtracted) reveals that the observed modulation is due to the nearby ^{7}Li nuclei, i.e., we find the signal exactly at the ^{7}Li Larmor frequency 5.8 MHz. The second peak at around 11 MHz is due to the double ^{7}Li frequency.[34] This result supports the suggestion that the observed narrow component of the ESR signal arises from the paramagnetic center whose wave function is at low temperatures localized in the vicinity of Li nuclei.

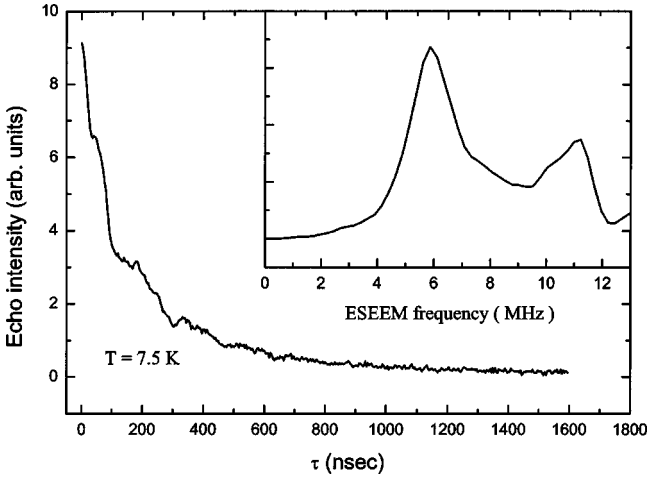

FIG. 10. A two-pulse echo intensity as a function of the pulse separation τ in $Li_x nMoS_2$ at $T=7.5$ K. The inset shows a Fourier transform of the observed modulation of the echo-decay curve. Two well-defined peaks are found: the strongest one at the expected ^{7}Li resonance ($\nu_L=5.8$ MHz) and the second one at the double ν_L frequency.

IV. DISCUSSION

One of the motivations for this work has been to understand why there is such a large irreversible capacity during the first electrochemical doping cycle (Fig. 2). The advantage of the ESR technique is that it is sensitive to changes on a local scale rather than on the average microscopic properties. However, the ESR data presented above point to a very complex and most probably inhomogeneous nature of electrochemically doped $n\mathrm{MoS_2}$. It is known for a long time, that in layered MoS_2 phases after intercalation of Li^+ ions into the host structure several different chemical reactions can happen leading eventually even to a partial amorphization of the sample. For instance it is suggested that Mo atoms can form clusters in layered MoS_2 phases during Li intercalation.[35–37] And there is intriguing presence of iodine in the $n\mathrm{MoS_2}$ which is believed to react with the intercalated Li on contact. The presence of such defects introduces disorder, which can largely influence the low-temperature electronic properties of doped $n\mathrm{MoS_2}$ and even disorder induced localization (i.e., of Anderson type) of otherwise delocalized electrons can take place. Because of the structural imperfections is the doping of $n\mathrm{MoS_2}$ most probably highly inhomogeneous. Electrons then find themselves in a very disordered environment where the local potential varies randomly. Such a system is in 3D usually described as a ''Fermi glass'' where for low temperatures and exciton energies small compared to the Fermi energy, the electrons may be viewed as forming a gas of localized quasiparticles.[38,39] Although additional transport, frequency-dependent ESR and SQUID magnetization measurements are needed to get deeper insight into the low-temperature physics of $Li_x nMoS_2$ we try to give here at least a tentative picture of the ground-state based on the present measurements.

The ESR spectrum of $Li_x nMoS_2$ consists of two components, a narrow and a broad one. We stress that the two components of the $Li_x nMoS_2$ ESR spectra are clearly distinguished over the entire temperature range. This suggests that the two different paramagnetic centers, responsible for the two different ESR components, are not interacting with each other and are most probably spatially separated. In what follows we'll therefore try to explain the origin and the nature of each component separately.

A. Discussion of the broad ESR component

Let us first discuss the temperature evolution of the main broad ESR component. We described in preceding section that the g-factor value of this line at room temperature is $g_2 \sim 2.15$ and that the corresponding linewidth is around 800 G. A similar line has been observed also in doped layered MoS_2 and we are thus tempted to assign this line to the MoS_2 system. We find at least two additional strong arguments for this assignment. First, during the electrochemical doping of the material we noticed that the amount of Li, which can be inserted into the ultrasonically dispersed $n\mathrm{MoS_2}$ (0.5 Li per MoS_2) is much smaller than the amount of Li that can be inserted into as-prepared $n\mathrm{MoS_2}$ (on average 2.3 Li per MoS_2). The ESR signal follows this behavior: the major broad ESR component is significantly weaker in doped dispersed $n\mathrm{MoS_2}$ samples. Li^+ ions can be either intercalated into the MoS_2 nanotubes (intratubular sites) or into the channels between the individual nanotubes (intertubular sites). The main effect of the dispersion of $n\mathrm{MoS_2}$ material is to reduce the relative volume of intertubular sites, compared to intratubular ones. The fact that the amount of Li^+, which can be inserted into the material, is dramatically reduced in dispersed samples strongly suggests that most of the Li^+ ions occupy intertubular sites. It also suggests that the broad ESR line is connected with the same intercalation process.

Further support for the suggestion that the broad ESR component is connected with the $n\mathrm{MoS_2}$ electronic system comes from the air sensitivity of the ESR signal. The decay of the broad ESR signal can be modeled with

$$I_{ESR}=I_0(1-\sqrt{t/t_0}). \tag{1}$$

Here I_0 is the initial ESR intensity before exposing the sample to air and t_0 is a characteristic time constant. We note here that such square-root time dependence is characteristic of diffusion processes in one dimension. This result is in agreement with the assumption that the broad component of the ESR signal is due to the Li intercalation into one-dimensional channels between $n\mathrm{MoS_2}$ as suggested earlier from the electrochemical and ESR results on dispersed sample. It also suggests that the sample is remarkably air stable. We attribute this stability to a particular one-dimensional porous structure of bundles of $n\mathrm{MoS_2}$ with a very selective pore sizes. As mentioned in the introduction, the pore size in a bundle of $n\mathrm{MoS_2}$ is just large enough to permit the diffusion of small Li^+ ions into the material. However, it strongly restricts the diffusion of larger moisture molecules in the host material. This dramatically slows down the degradation process of $Li_x nMoS_2$ and may be useful if MoS_2 nanotubes are used for the electrochemical storage of energy. A likely reason for the air sensitivity of the sample

is a water uptake by intercalated Li as suggested to be the case in alkali metal intercalated fullerenelike MS_2 (M=W,Mo)nanoparticles.[28]

In view of the above assignment of the broad ESR component it is interesting to compare the observed ESR spectra with the ESR signals observed in different layered MoS_2 phases. We note, that many different paramagnetic ESR signals in various layered $MoS_{2+x}O_y$ systems have been identified.[40–42] Quite generally they can be divided into three different[43,44] groups: (i) electron hole center localized on a sulfur atom,[45] (ii) Mo(V) center surrounded by sulfur atoms,[43] and (iii) Mo(V) center surrounded by oxygen atoms. None of these centers really correspond to our signal. Both their g factors as well as the linewidth do not match the observed broad ESR component in Li_xnMoS_2. On the other hand, the measured broad ESR line resembles the one measured in Rb saturated layered MoS_2 where it has been identified as the d-band conduction electrons of the host 2H-MoS_2, which have been donated to Mo derived bands by the Rb intercalant.[46] It has been theoretically suggested[47] that the Mo d states especially dominate the upper valence-band and the lower conduction-band edges.

The assignment of our broad ESR signal to conducting-electron-spin resonance (CESR) of Li donated electrons in the Mo d-state derived conducting band of $nMoS_2$ is thus a very likely possibility. Structural disorder, static or dynamic, can on the other hand have a large impact on the electronic structure and consequently on the ESR signal. Among many different models for the broad ESR component we find two main candidates: (a) broad ESR signal is due to the conducting electrons coupled to defects and (b) random exchange model. Below we describe arguments for the applicability of these two models to broad ESR component of Li_xnMoS_2.

1. CESR model

The estimated value of the ESR susceptibility of the broad ESR component is very large and as such it must reflect topology of the sample or/and high density of states in our sample or/and possible correlation effects. Van Hove singularities as a result of the quantum confinement of electrons in the radial and circumferential directions of the nanotubes have been theoretically predicted[48] and experimentally observed in carbon nanotubes.[49] They were also observed in molybdenum selenide molecular wires.[50] It is thus reasonable to expect Van Hove singularities in the local density of states also in or $nMoS_2$ nanotubes especially due to the rather small radius of our nanotubes. The Pauli spin susceptibility, which is in metallic sample proportional to the density of states at the Fermi level, can then be enhanced if the Fermi-level coincides with the singularity. These singularities are extremely peaked and a large temperature dependence of the Pauli susceptibility is expected—larger than observed in this experiment.

Traditionally, it is assumed that the observed CESR is broadened and shifted by the so-called Elliot mechanism.[51] Within this model the CESR linewidth normally decreases with decreasing temperature. This is obviously not the case for the broad ESR line in Li_xnMoS_2. Furthermore, assuming a 1D electronic structure in Li_xnMoS_2, the spin-orbit scattering should be reduced as the momentum space into which the electrons can scatter is also reduced. One thus expects narrower lines.

Broadening of the CESR line at low temperatures in metals can be achieved by assuming the presence of defects. If the defects are paramagnetic then the expected temperature dependence of the ESR linewidth[52] is

$$\Delta H_{pp} \propto 1/(\chi^2_{cond.} T). \tag{2}$$

An attempt to fit the temperature dependence of the linewidth is shown by dotted line in Fig. 7 using the experimentally determined susceptibility. Although the fit is not ideal it describes well the overall temperature dependence of the measured ESR linewidth.

On the other hand the defects can be also topological (without magnetic moment), which can act as a trapping center for conducting electrons. The effective ESR linewidth within this model can be expressed as

$$\Delta H_{pp} = C(T)\Delta H_t + [1 - C(T)]\Delta H_c, \tag{3}$$

where ΔH_t and ΔH_c denote the ESR linewidth of the trapped and conducting states, respectively. $C(T)$ is the relative population of the trapped spin state and has been calculated in Ref. 53 to be $C(T)=p/[p+(1-p)\exp(-E_b/kT)]$. Here E_b is the trapping energy and p concentration of the traps. Fit (solid line in Fig. 7) lead to the binding-energy $E_b = 134 \pm 7$ K and $p = 0.24 \pm 0.01$. We note that the concentration of trap centers is quite high suggesting a strongly disordered structure of Li_xnMoS_2.

These defects can be a result of various chemical reactions during the electrochemical doping. However, we suggest that they can be also spontaneously formed on charged $nMoS_2$. A very large susceptibility suggests a very high density of states at the Fermi level and one would thus expect that the system is very unstable against any lattice distortion and a formation of a new ground state with a lower energy. It may well be that the defects, we discussed above, are in fact intrinsic and are spontaneously formed in some sections of doped $nMoS_2$ as a result of the ground-state instability.

The CESR model thus can describe our data if a very high susceptibility is ascribed to the extremely high density of states and the temperature dependence of the CESR linewidth is due to the high concentration of defects.

2. Random exchange model

It is well known that layered MoS_2 phases undergo a significant structural transformation upon Li intercalation. One of the consequences of the amorphization process is that Mo can form also clusters in the so called ''diamond-chain'' scheme.[36,37,54] Something similar may happen also in Li_xnMoS_2 where the effective nanotube length is decreased (Mo finite length chains) and the $nMoS_2$ become disordered. As the Mo-Mo distance in such a case decreases we can expect that the two Mo^{3+} ($S=3/2$) will be coupled together by the exchange interaction $\mathcal{H}_E = J\vec{S}_1 \cdot \vec{S}_2$. Due to the local disorder the exchange coupling constant J may randomly vary from site to site. Such a situation is usually described within the random-exchange Heisenberg antiferromagnetic

chain model first studied in detail by Bondeson and Soos.[55,56] The appropriate Hamiltonian is then given by

$$\mathcal{H}=\sum_n Jx_n\vec{S}_n\cdot\vec{S}_{n+1}+g\mu_B H\sum_n S_n^z. \quad (4)$$

Here x_n is a random variable and represents a disorder in the exchange interactions. A crossover from a Bonner-Fisher type temperature dependence of the spin susceptibility at high temperatures to power-law ($\chi\propto T^{-\alpha}$ with $0\leqslant\alpha\leqslant 1$) dependence is predicted at low temperatures. According to our measurements this crossover would happen at around 50 K. The ESR lineshape is a sum of contributions from tube segments of different length

$$I(\omega)=\frac{1}{N}\sum_{k=1}^{N}\chi_k\frac{\Gamma_k}{\pi(\omega^2+\Gamma_k^2)}, \quad (5)$$

where χ_k and Γ_k are the susceptibility and the linewidth of the tube segment k. N is simply a number of different segments. This model predicts a gradual increase in the ESR linewidth with decreasing temperature with a characteristic $\Delta H\propto\ln(T_0/T)$ at temperatures below the crossover.[57] As this behavior should be observed well below 50 K, where due to the large broadening we cannot detect broad ESR component anymore, we cannot confirm the random-exchange model in Li_xnMoS_2 on the basis of these measurements.

However, the observations, i.e., the temperature dependence of the susceptibility and the linewidth, are in general in agreement with the random-exchange Heisenberg chain model. To make a more firm conclusion on the origin of the broad ESR line, additional transport, magnetic or frequency dependent ESR measurements will have to be performed.

B. Discussion of the origin of the narrow ESR component

Although the intensity of the narrow ESR component represents only few percents of the total ESR intensity, this line appears in every doped $nMoS_2$ sample while it is not present in undoped nanotubes. We therefore believe that it emerges during the electrochemical charging of $nMoS_2$ and therefore deserves to be studied as well.

The ESR data extracted from the measurement of the narrow ESR component may be at first glance confusing. First, the ESR susceptibility data can be reasonably fit in the entire temperature range to a sum of two contributions,

$$I_{ESR}=\left[\chi_P^0+\left(\frac{\partial\chi_P}{\partial T}\right)T\right]+\frac{C}{T-\theta}. \quad (6)$$

Here the first two terms in the brackets are due to weakly temperature-dependent Pauli-like term. We assumed only a weak linear decrease with decreasing temperature. The last term is the Curie-like contribution to the total ESR susceptibility of the narrow component. This model fits the experimental data over the entire temperature range (Fig. 9). The numerical determination of the Pauli susceptibility χ_P^0 and the Curie constant C is impossible as the mass of the part of the sample connected with this signal is impossible to determine. We find that θ is very close to 0 (i.e., unconstrained fit lead to $\theta=-2\pm0.5$ K).

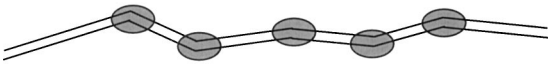

FIG. 11. Schematically presented view of the Li_xnMoS_2 ground state. Please note that the ''defects'' (gray circles) ''cut'' the nanotube to shorter segments.

The temperature dependence of the linewidth of the narrow ESR component on the other hand shows only a gradual increase with decreasing temperature [Fig. 9(b)]. Again the Elliot relaxation mechanism[51] is obviously not appropriate. We note, however, that quenching of the Elliot relaxation mechanism, change of the ESR lineshape to symmetrical Lorentzian with the electronic spin susceptibility following Curie law rather than Pauli-like behavior is theoretically predicted for small enough metallic particles or systems with small physical dimensions.[58–60]

We can consider a number of possible scenarios, which could lead to such effects. The first possibility is that due to the finite size of the MoS_2 nanotubes the electrons donated from the intercalated Li are confined within the diameter of the nanotube. However, in such a case it is difficult to understand Dysonian lineshape of the narrow ESR component observed between room temperature and 100 K.[61] Alternatively, small metallic Li dendrites might also form during the charge or discharge processes. However, these would be expected to be very reactive to moisture, while apparently they are not: the narrow line is only very weakly airsensitive, even less so than the broad line. Another possibility, which we consider most likely, is the formation of small spin clusters on the NTs themselves. The asymmetric lineshape may then reflect the distribution of cluster sizes contributing to the ESR signal. These clusters may be coupled to itinerant electron spins on the NTs, giving rise to a T-dependent lineshape.

V. CONCLUSIONS

In conclusion, ESR measurements on doped and undoped MoS_2 nanotubes show rather complicated behavior, which we attribute to their strongly one-dimensional character. Undoped $nMoS_2$ material has no ESR signal. On the other hand Li_xnMoS_2 consistently shows two different ESR signals over the entire temperature range, suggesting two different—most probably spatially separated paramagnetic species. The majority of Li^+ ions appear to be intercalated in 1D channels—most probably in between the MoS_2 nanotubes.[60]

The doped material is only moderately air sensitive. The degradation of the doped materials is characterized by one-dimensional diffusion processes. The insertion of Li^+ ions into the channels between MoS_2 nanotubes is accompanied by a charge transfer to the Mo d-state derived bottom of the conducting band of MoS_2 nanotube, suggesting that Mo d electrons are responsible for the ESR signal.

A view of the low-temperature ground state of the Li_xnMoS_2 is schematically presented on Fig. 11. Many defects may form during MoS_2 nanotube growth and the inter-

calation process. These defects are suggested to have an important effect on the low-temperature properties of Li_xnMoS_2, effectively they decrease the spin correlation length. The exact nature and origin of defects is unknown at present. Defects can be extrinsic in origin as a result of various chemical reactions of Li with the host material and can be either paramagnetic or nonmagnetic. We also discussed the possibility of the spontaneous formation of spin cluster defects as a result of the intrinsically high susceptibility of the material. Our ESR results are compatible both with CESR and the random-exchange Heisenberg chain model, but further experiments, particularly on resistivity, are needed to clarify this point. Nevertheless it seems that the Li_xnMoS_2 system exists in a highly disordered state and does not undergo a transition to any ordered low-temperature ground state in spite of the large spin susceptibility—which is highly surprising. Finally, we remark that regardless of the effect of defects, it seems that the MoS_2 nanotubes are significantly superior to the layered MoS_2 phases in terms of Li electrochemical storage capacity and consequently appear to be promising new material for Li-ion battery electrodes.

ACKNOWLEDGMENTS

A.D. acknowledges financial support of NATO through SfP Grant No. 976913.

[1] S. Iijima, Nature New Biol. **354**, 56 (1991).
[2] J. Voit, Rep. Prog. Phys. **57**, 977 (1994).
[3] J.M. Luttinger, J. Math. Phys. **4**, 1154 (1963).
[4] M. Bockrath, D.H. Cobden, J. Lu, A.G. Rinzler, R.E. Smalley, L. Balents, and P.L. McEuenn, Nature (London) **397**, 598 (1999).
[5] Z. Yao, H.W.J. Potsma, L. Balents, and C. Dekker, Nature (London) **402**, 273 (1999).
[6] M. Grayson, D.C. Tsui, L.N. Pfeiffer, K.W. West, and A.M. Chang, Phys. Rev. Lett. **86**, 2645 (2001).
[7] B. Gao, A. Kleinhammes, X.P. Tang, C. Bower, L. Fleming, Y. Wu, and O. Zhou, Chem. Phys. Lett. **307**, 153 (1999).
[8] A. Cleye, S. Rahman, J.E. Fischer, A. Sirenko, G.U. Sumanasekera, and P.C. Eklund, Chem. Phys. Lett. **333**, 16 (2001).
[9] C. Bower, A. Kleinhammes, Y. Wu, and O. Zhou, Chem. Phys. Lett. **288**, 481 (1998).
[10] K. Metenier, L. Duclaux, H. Gaucher, J.P. Salvetat, P. Lauginie, S. Bonnamy, and F. Beguin, *Electronic Properties of Novel Materials-Progress in Molecular Nanostructures*, edited by H. Kuzmany, J. Fink, M. Mehring, and S. Roth, AIP Conf. Proc. No. **442** (AIP, Woodburg, NY, 1998), p. 51.
[11] H. Shimoda, B. Gao, X.P. Tang, A. Kleinhammes, L. Fleming, Y. Wu, and O. Zhou, Phys. Rev. Lett. **88**, 015502 (2001).
[12] N.G. Chopra, N.G. Chopra, R.L. Luyken, K. Cherrey, V.H. Crespi, M.L. Cohen, S.G. Louie, and A. Zettl, Science **269**, 966 (1995).
[13] See for instance D. Golberg, Y. Bando, K. Kurashima, and T. Sato, J. Nanosci. Nanotechnol. **1**, 49 (2001); S. Okada, S. Saito, and A. Oshiyama, Phys. Rev. B **64**, 201303 (2001).
[14] M. Niederberger, H.-J. Muhr, F. Krumeich, F. Bieri, D. Günther, and R. Nesper, Chem. Mater. **12**, 1996 (2000).
[15] A. Dobley, K. Ngala, S. Yang, P.Y. Zavalij, and M.S. Whittingham, Chem. Mater. **13**, 4382 (2001).
[16] R. Tenne, L. Margulis, M. Genut, and G. Hodes, Nature (London) **360**, 444 (1992).
[17] L. Margulis, G. Salitra, R. Tenne, and M. Talianker, Nature (London) **365**, 113 (1993).
[18] M. Remškar, Z. Škraba, F. Cleton, R. Sanjines, and F. Lévy, Appl. Phys. Lett. **74**, 3633 (1999).
[19] M. Remškar, Z. Škraba, M. Regula, C. Ballif, R. Sanjinés, and F. Lévy, Adv. Mater. **10**, 246 (1998).
[20] J. Chen, N. Kuriyama, H. Yuan, H.T. Takeshita, and T. Sakai, J. Am. Chem. Soc. **123**, 11 813 (2001).
[21] M. Remškar, A. Mrzel, Z. Škraba, A. Jesih, M. Čeh, J. Demšar, P. Stadelmann, F. Lévy, and D. Mihailović, Science **292**, 479 (2001).
[22] M. S. Dresselhaus, G. Dresselhaus, and P. C. Eklund, *Science of Fullerenes and Carbon Nanotubes* (Academic, New York, 1996).
[23] M.S. Whittingham, J. Solid State Chem. **29**, 303 (1979).
[24] D. Guyomard, in *New Trends in Electrochemical Technology: Energy Storage Systems for Electronics*, edited by T. Osaka and M. Datta (Gordon and Breach, New York, 2000), Chap. 9, p. 253.
[25] As grown swatches of MoS_2 nanotubes were dissolved in ethanol and then ultrasonically dispersed. Atomic force microscopy was then used to confirm that the obtained material made of primarily of individual nanotubes or smaller bundles of MoS_2 nanotubes.
[26] R. Dominko, D. Arčon, A. Mrzel, A. Zorko, P. Cevc, P. Venturini, M. Gaberščček, M. Remškar, and D. Mihailović, Adv. Mater. **14**, 1531 (2002).
[27] R. Dominko, M. Gaberščček, P. Venturini, D. Arčon, A. Mrzel, M. Remškar, S. Pejovnik, and D. Mihailović, *Structural and Electronic Properties of Molecular Nanostructures*, edited by H. Kuzmany, J. Fink, M. Mehring, and S. Roth, AIP Conf. Proc. No. **633** (AIP, Melville, New York, 2002), p. 624.
[28] A. Zak, Y. Feldman, V. Lyakhovitskaya, G. Leitus, R. Popovitz-Biro, E. Wachtel, H. Cohen, S. reich, and R. Tenne, J. Am. Chem. Soc. **124**, 4747 (2002).
[29] M. Gaberščček, M. Bele, J. Drofenik, R. Dominko, and S. Pejovnik, Electrochem. Solid-State Lett. **3**, 171 (2000).
[30] See for instance *Modern Batteries*, edited by C. A. Vincent and B. Scrosati (Wiley, New York, 1997), p. 198–242.
[31] See for instance R.B. Somoano, V. Hadek, and A. Rembaum, J. Chem. Phys. **58**, 697 (1973).
[32] F.J. Dyson, Phys. Rev. **98**, 349 (1955).
[33] J. R. Pilbrow, *Transition Ion Electron Paramagentic Resonance* (Clarendon, Oxford, 1990), p. 440.
[34] A. Schweiger and G. Jeschke, *Principles of Pulse Electron Paramagnetic Resonance* (Oxford University Press, Oxford, 2001).
[35] K.E. Dungey, M.D. Curtis, and J.E. Penner-Hahn, Chem. Mater. **10**, 2152 (1998).
[36] X. Rocquefelte, F. Boucher, P. Gressier, G. Ouvrard, P. Blaha, and K. Schwarz, Phys. Rev. B **62**, 2397 (2000).
[37] V. Petkov, S.J.L. Billinge, P. Larson, S.D. Mahanti, T. Vogt, K.K.

Rangan, and M.G. Kanatzidis, Phys. Rev. B **65**, 092105 (2002).
[38] R. Freedman and J.A. Hertz, Phys. Rev. B **15**, 2384 (1977).
[39] K.A. Müller, T. Penney, M.W. Shafer, and W.J. Fitzpatric, Phys. Rev. Lett. **47**, 138 (1981).
[40] Y. Bensimon, P. Belougne, J.C. Giunti, and J.V. Zanchetta, J. Phys. Chem. **88**, 2754 (1984).
[41] L. Busetto, A. Vaccari, and G. Martini, J. Phys. Chem. **85**, 1927 (1981).
[42] K.S. Liang, S.P. Cramer, D.C. Johnston, C.H. Chang, A.J. Jacobson, J.P. Deneuville, and R.R. Chianelli, J. Non-Cryst. Solids **42**, 345 (1982).
[43] R. Berger and M. Haddad, Phys. Status Solidi B **163**, 463 (1991).
[44] B. Deroide, Y. Bensimon, P. Belougne, and J.V. Zanchetta, J. Phys. Chem. Solids **52**, 853 (1991).
[45] H.E. Radford, and F.O. Rice, J. Chem. Phys. **33**, 774 (1960).
[46] S. Bandow, Y. Maruyama, X.X. Bi, R. Ochoa, J.M. Holden, W.T. Lee, and P.C. Eklund, Mater. Sci. Eng., A **204**, 222 (1995).
[47] G. Seifert, H. Terrones, M. Terrones, G. Jungnickel, and T. Frauenheim, Phys. Rev. Lett. **85**, 146 (2000).
[48] J.-C. Charlier and Ph. Lambin, Phys. Rev. B **57**, R15 037 (1998).
[49] P. Kim, T.W. Odom, J.-L. Huang, and C.M. Lieber, Phys. Rev. Lett. **82**, 1225 (1999).
[50] L. Venkataraman and C.M. Lieber, Phys. Rev. Lett. **83**, 5334 (1999).
[51] R.J. Elliot, Phys. Rev. **96**, 266 (1954); Y. Yafaet, Solid State Phys. **14**, 1 (1963).
[52] A. Wolter, U. Fasol, R. Jappelt, and E. Dormann, Phys. Rev. B **54**, 12 272 (1996).
[53] M. Nechtschein, F. Devreux, F. Genoud, M. Guglielmi, and K. Holczer, Phys. Rev. B **27**, 61 (1983).
[54] J. Guillevic, J.Y. Le Marouille, and J. Grandjean, Acta Crystallogr., Sect. B: Struct. Crystallogr. Cryst. Chem. **B30**, 111 (1974).
[55] Z.G. Soos and S.R. Bondeson, Solid State Commun. **35**, 11 (1980).
[56] S.R. Bondeson and Z.G. Soos, Phys. Rev. B **22**, 1793 (1980).
[57] Z.G. Soos and S.R. Bondeson, Solid State Commun. **39**, 289 (1980).
[58] R. Kubo, J. Phys. Soc. Jpn. **17**, 975 (1962).
[59] A. Kawabata, J. Phys. Soc. Jpn. **29**, 902 (1970).
[60] S. Sato, J. Phys. Soc. Jpn. **59**, 1366 (1990).
[61] A. Grupp (private communication).